

Article

CO₂ Curing of Ca-Rich Fly Ashes to Produce Cement-Free Building Materials

Mustafa Cem Usta ^{1,*}, Can Rüstü Yörük ¹, Mai Uibu ¹, Tiina Hain ², Andre Gregor ¹ and Andres Trikkel ¹ 

¹ Department of Materials and Environmental Technology, Tallinn University of Technology, 19086 Tallinn, Estonia; can.yoruk@taltech.ee (C.R.Y.); mai.uibu@taltech.ee (M.U.); andre.gregor@ttu.ee (A.G.); andres.trikkel@taltech.ee (A.T.)

² Department of Civil Engineering and Architecture, Tallinn University of Technology, 19086 Tallinn, Estonia; tiina.hain@ttu.ee

* Correspondence: mustafa.usta@taltech.ee

Abstract: In this study, fly ash (FA) compacts were prepared by accelerated carbonation as a potential sustainable building material application with the locally available ashes (oil shale ash (OSA), wood ash (WA) and land filled oil shale ash (LFA)) of Estonia. The carbonation behaviour of FAs and the performance of 100% FA based compacts were evaluated based on the obtained values of CO₂ uptake and compressive strength. The influence of different variables (compaction pressure, curing temperature, CO₂ concentration, and pressure) on the CO₂ uptake and strength development of FA compacts were investigated and the reaction kinetics of the carbonation process were tested by different reaction-order models. A reasonable relation was noted between the CO₂ uptake and compressive strength of the compacts. The porous surface structure of the hydrated OSA and WA compacts was changed after carbonation due to the calcite formations (being the primary carbonation product), especially on portlandite crystals. The increase of temperature, gas pressure, and CO₂ concentration improved the CO₂ uptake levels of compacts. However, the positive effect of increasing compaction pressure was more apparent on the final strength of the compacts. The obtained compressive strength and CO₂ uptake values of FA compacts were between 10 and 36 MPa and 11 and 13 wt%, respectively, under various operation conditions. Moreover, compacts with mixed design (OSA/LFA and WA/LFA) resulted in low-strength and density compared to the single behaviour of OSA and WA compacts, yet a higher CO₂ uptake was achieved (approximately 15% mass) with mixed design. The conformity of Jander equation (3D-diffusion-limited reaction model) was higher compared to other tested reaction order models for the representation of the carbonation reaction mechanism of OSA and WA. The activation energy for OSA compact was calculated as 3.55 kJ/mol and for WA as 17.06 kJ/mol.

Keywords: fly ash utilization; accelerated carbonation; building materials



Citation: Usta, M.C.; Yörük, C.R.; Uibu, M.; Hain, T.; Gregor, A.; Trikkel, A. CO₂ Curing of Ca-Rich Fly Ashes to Produce Cement-Free Building Materials. *Minerals* **2022**, *12*, 513. <https://doi.org/10.3390/min12050513>

Academic Editors: Carlos Hoffmann Sampaio, Wesley Monteiro Ambros and Bogdan Grigore Cazacliu

Received: 22 March 2022

Accepted: 18 April 2022

Published: 21 April 2022

Publisher's Note: MDPI stays neutral with regard to jurisdictional claims in published maps and institutional affiliations.



Copyright: © 2022 by the authors. Licensee MDPI, Basel, Switzerland. This article is an open access article distributed under the terms and conditions of the Creative Commons Attribution (CC BY) license (<https://creativecommons.org/licenses/by/4.0/>).

1. Introduction

Since the manufacture of cement, CO₂ emissions of the cement industry have been on a large scale and the direct CO₂ intensity of cement production increased 1.8% annually during 2015–2020 [1,2]. Cement production is estimated to increase even more, and thus reducing CO₂ emissions while producing enough cement to meet demand will be challenging until 2030 due to EU restrictions [1,2]. Carbon capture and storage at cement production plants could be a solution to this problem, yet there is no commercially available full-scale application until today [3,4]. Researchers throughout the world have been searching for alternatives to cement among waste materials to cut cement dependency and lower the related CO₂ emissions [3,5]. Primarily, fly ash (FA), which is generally disposed of in landfills, has always been an alternative to cement, as it is considered a supplementary cementitious material which provides one of the most feasible routes for concrete production with reduced CO₂ emissions [6].

The suitability of FA depends on the chemical and mineralogical composition such as the content of siliceous or siliceous-and-aluminous material, lime, portlandite, and its physical properties [7]. Although FA has several advantages on concrete properties, there are still several drawbacks that limit the applications on a big scale due to the reduction of mechanical properties of the concrete and its durability. As FA amounts increase in concrete, the mechanical properties of the concrete decrease, which means that remarkable replacement ratios are infeasible in today's construction applications [6–8].

With the increase of environmental consciousness, the building sector is evolving with the integration of circular economy concepts for better waste utilization and zero carbon emissions. Mineral carbonation is at the forefront due to recent progress when it comes to the utilization of both industrial alkaline waste materials and CO₂ gas without using traditional binders towards sustainable construction materials [9–13]. Considering the vast amount of ashes generated from both fossil and renewable fuels, and for the applications of non-traditional construction materials, the usage of FAs via carbonation activation could be a promising alternative for producing cement-free building materials.

Calcium (Ca) and magnesium (Mg) are considered as two of the most dominant and reactive (with respect to CO₂) alkaline earth metals found in industrial residues [14–16]. Based on the chemical composition of the ashes, Ca and Mg-rich FAs are found to be potential candidate materials for CO₂ mineralization due to their high alkalinity. The average CO₂ uptake level of most of the alkaline solid wastes including ashes can also be directly connected to the contents of Ca and Mg [12,15,17].

In Estonia, Ca-rich ashes; oil shale ash (OSA), and wood ash (WA) are widely produced, constituting more than 70% of the total residues generated by power plants. As a result of the past industrial processes involving oil shale (OS) combustion and retorting (approximately 100 years) and due to the limited ash utilization applications, there are more than 300 million tonnes of land filled OS ash (LFA) in plateau-like waste depositories [18,19]. The ash problem and CO₂ emissions, which are elevated by high carbonate content in OS, are key issues undermining the long-term sustainability of the energy sector of Estonia. Therefore, valorisation of the ashes in environmentally sound applications is of clear strategic interest to the country. The utilization of local alkaline waste streams together with CO₂ via mineral carbonation can contribute to the circular economy and sustainable development.

In an early investigation on typical residues from the OS industry of Estonia, a mineral carbonation approach was studied for the first-time to evaluate the suitability and reactivity of available OSAs. The preliminary findings on CO₂ uptake (up to 9%) were promising, reflecting on the improved strength (20–40 MPa) as a result of mainly the carbonation of Ca(OH)₂ forming CaCO₃ crystals [20]. With respect to this positive outcome, principally OSA, WA, and LFA could be useful waste materials for both capture and permanent sequestration of CO₂ through the formation of CaCO₃, as these waste streams contain high amounts of calcium mainly due to the presence of free lime and portlandite.

It is also known that the formation of the CaCO₃ phase has a positive effect on construction materials because of the increased density through a filling effect, which improves the microstructure, lowers the permeability, and improves strength [21,22]. This behaviour of strength development has been studied with different waste materials including steel slag, blast furnace slag, construction demolition waste, municipal solid waste, coal combustion FA, and ashes from wood and peat combustion under controlled process conditions [21–26]. In most of these studies, carbonation tests of compacted or granulated pellets, blocks, etc., were carried out both in a CO₂ rich and lean atmosphere for modelling flue gas (FG) curing as well. It has been shown that there is a direct relation with the CO₂ uptake level and the strength gain in compacts. Since carbonation is a dynamic process involving transport of CO₂ through a compact body and dissolution of Ca, studies have shown that the extent of carbonation reactions are influenced by various parameters (reaction time, curing temperature and pressure, relative humidity (RH), CO₂ concentration, physical properties of residues etc.) [12,16,22]. However, both an excess and a scarcity of the above-mentioned

parameters can result in negative effects for the entire process relating to CO₂ uptake and strengthening of the compacts.

Additionally, the achievement of the most effective CO₂ curing process and improvement in mechanical properties of compacts are highly dependent on the chemical composition and mineralogy of industrial residues [17]. It is important to bear in mind that these operation parameters must be optimized for each waste, as well as the relevant process stages for homogeneous carbonation and to lower the operational energy costs. Therefore, there is a necessity to address a research study focusing on the utilization of Ca-rich FAs in an Estonian context (OSA, WA, LFA) to gain in-depth understanding of the impacts of operation conditions during CO₂ curing to produce cement-free building materials.

The main aim of the study is to evaluate and characterize the carbonation behaviour of selected ashes based on the obtained values of CO₂ uptake and compressive strength while providing a comparative crosscheck on the rate of carbonation and mechanical performance of compacts. This study undertakes parametric investigations to understand the effects of compaction pressure, curing temperature, CO₂ concentration, and pressure on the carbonation extent and related strength development of the compacts. The reaction kinetics of the carbonation process were also tested by different reaction-order models in order to identify the carbonation reaction behaviour of Ca-rich FAs. Furthermore, the preliminary tests with LFA and impacts of mixing LFA with OSA and WA are presented for future perspectives of potential sustainable building material applications with local available ashes.

2. Materials and Methods

2.1. Materials

Three different types of ash samples were selected from Estonia (OSA, WA, and LFA). OSA was obtained from *Auvere Power Plant* [27], which is operated by the direct combustion of OS in CFB boiler for power production, and ash was collected from the electrostatic precipitators. WA was obtained from *Utilitas District Heating Plant* [28] which is operated by forestry wood (a mix of pine chips and bark residues) and ash was collected from bag filters located in the post-combustion zones of the grate combustor. The LFA samples were taken from a drill core made on the rim of the ash disposal site at *Eesti Power Plant* [29], north-eastern Estonia (Figure 1). The selected LFA is the ash taken from the depths of 32.4–32.6 m, where mainly burnt OS FA residues exist from electricity production without including shale oil processing residues.



Figure 1. Drill core from ash disposal site at the Eesti Power Plant, north-eastern Estonia.

2.2. Characterization of Materials (Initial and Compacts)

All samples were obtained in fine fractions, which did not require pre-treatment (drying, milling, or grinding etc.) except the LFA samples, which were milled by Tartu University. Mean samples were taken from each collected ashes, and a size fraction below 200 µm (by sieving) was used for material characterization and further sample preparation. The physical characterization of the selected waste streams included particle size distribution (PSD) measurements. Horiba Laser Scattering instrument (LA-950) (Kyoto,

Japan) was used for PSD measurement (with ethanol suspension). The BET-N₂ sorption method was used to measure the specific surface area (SSA) with Kelvin 1042 sorptiometer (Tallinn, Estonia). The chemical and mineralogical characterization of the selected waste streams included X-ray fluorescence (XRF) and X-ray diffraction (XRD) analyses with Bruker S4 Pioneer (Karlsruhe, Baden-Württemberg, Germany) and Bruker D8 (Karlsruhe, Baden-Württemberg, Germany) diffractometers, respectively, using Cu K α radiation with a Göbel mirror monochromator and LynxEye positive sensitive detector over a 2°–70° 2 θ range. The thermogravimetric (TGA) and mass spectrometric (MS) analysis were also carried out to obtain thermal characterization of both carbonated and un-carbonated compacted samples (mainly for the calculation of CO₂ uptake) by using the Setaram Labsys 2000 thermoanalyzer (Geneva, Switzerland) (10 K/min, sample mass: 20 ± 1 mg, 21% O₂/79% Ar) with alumina (Al₂O₃) crucible. The SEM images of carbonated compacts were obtained from the polished samples using a ZEISS Evo MA 15 (Oberkochen, Baden-Württemberg, Germany) for the investigation of the microstructure. The mineralogical composition was determined using XRD analysis to compare mineralogical changes after carbonation curing. The compressive strength measurements were performed with Toni TechnikD-13355 (Berlin, Brandenburg, Germany). The measurements of pH were conducted according to EN 12457-2 on compacts. Tube test duration was 24 h with distilled water, 1/10 solid/liquid ratio, 32 rpm rotation speed, and 0–4 mm grain size particles were used. SevenGo Duo pH/Cond meter SG23 (Greifensee, Switzerland) was used for the pH measurements.

2.2.1. Physical Characterization

OSA, WA, and LFA samples have BET SSA of 5.8 m²/g, 11.9 m²/g, and 20.6 m²/g respectively, which can indicate higher carbonation ability for LFA compared to other ashes, since the carbonation reaction is promoted by the presence of a higher number of sites available in the initial material [30] (see Figure 2). Although the SSA of LFA and WA was higher than OSA, due to the phases formed during natural hydration and biomaterial nature of WA respectively, it was revealed that the median particle diameter is 79.2 μ m for LFA, 54.6 μ m for WA, and 23.4 μ m for OSA.

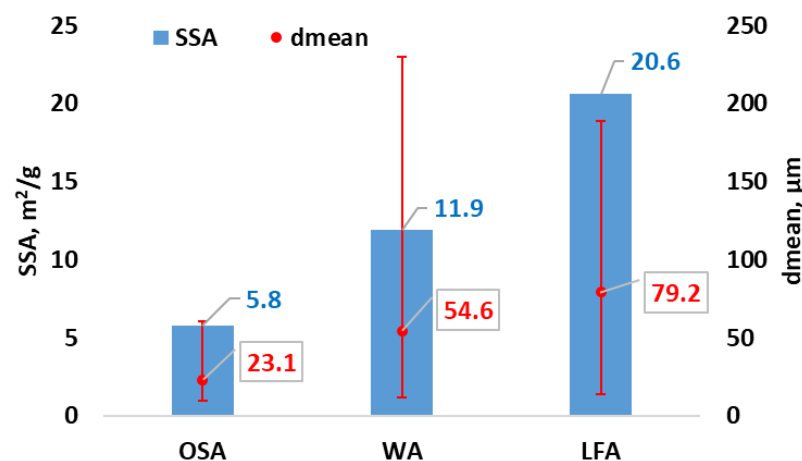


Figure 2. Average particle diameter (d_{mean}) and specific surface areas (SSA) of OSA, WA, and LFA samples.

2.2.2. Chemical Characterization

According to XRF analysis, all three types of samples were composed of mainly Ca and Si, adding up to 59–64% (see Table 1). The XRD analysis showed that OSA and WA contain a considerable amount of free lime (17–20%) with a small amount of portlandite (1.4–3%), which are supposed to be the main phases to react with CO₂ (see Table 2). Dicalcium silicate, 'C₂S', which is an important well-known component of clinker in cement industry, constitutes 13.9% of OSA and 4.1% of WA. Differently in LFA, hydration of CaO under

natural water produced $\text{Ca}(\text{OH})_2$, which constitutes 18% of the phases. Similarly, dicalcium silicates in LFA are also hydrated and formed CSH (Calcium silicate hydrate), which is composed of 45% of the phase composition due to atmospheric water reacting with the constituents of the ash in the disposal area.

Table 1. Chemical composition of OSA, WA, and LFA.

Component	OSA1	WA	LFA
SiO_2	29.38	18.08	17.38
Al_2O_3	9.58	2.73	4.13
TiO_2	0.578	0.19	0.21
Fe_2O_3	5.12	1.17	2.43
MnO	0.067	0.32	0.03
CaO	34.67	44.44	42.21
MgO	3.12	2.82	3.75
Na_2O	0.12	0.52	0.10
K_2O	3.91	7.69	0.81
P_2O_5	0.128	4.14	0.13
SO_3	4.96	4.35	4.97
L.O.I.	7.73	12.79	22.90

Table 2. Phase composition of OSA, WA, and LFA.

Component	OSA (%)	WA (%)	LFA (%)
Quartz	15	7.5	5
K-feldspar	14.2	3.2	3
Plagioclase	0.7	0	0
Mica	3.6	0	0
Calcite	9.8	27.7	3
Lime	17	20.3	0
Portlandite	1.4	3	18
Periclase	4.2	2.9	2
Anhydrite	9.3	0	0
C_2S	13.9	4.1	3
Merwinite	3.2	4.3	2
Akermanite	4.5	3.8	5
Sylvite	0	1.7	0
Arcanite	0	8.6	0
Hematite	2.3	0	0
Apatite	0	12.6	0
CSH (tobermerite)	0	0	45
Gypsum	0	0	2
Ettringite	0	0	2

Cement powders require the presence of C_2S in the clinkers for strength development in concrete. These materials react vigorously with water to produce the cement paste formed in the final product. Within the building industry, the term “pozzolan” covers all the materials that react with lime and water, producing calcium silicate and aluminates hydrates. All pozzolans must be rich in reactive silica or alumina plus silica [31]. SiO_2 , Al_2O_3 , and Fe_2O_3 constitute 22–45% of the samples of which are described as main constituents of pozzolans. An internal sulphate attack is a deterioration mechanism of concrete. High percentages of SO_3 in the cement increase the risk of delayed ettringite formation, which can lead to significant deterioration of the concrete structure [32]. ASTM C618 (Standard specification for coal FA use in concrete) limits the sulphate content of fly ash to 5% SO_3 when the material is to be used in concrete [33].

2.3. Sample Preparation and Carbonation Apparatus

OSA and WA were selected as the two main samples for planned experiments within this study. LFA was included only for preliminary evaluation and for its capabilities as a potential mix design with OSA and WA at a ratio of 50/50.

In the first step, the hydrated OSA and WA samples have been prepared with a liquid to solid ratio of 0.25 *w/v* and LFA has been prepared with the liquid to solid ratio of 0.15 *w/v* (to ensure $10 \pm 1\%$ moisture content for all samples before curing). The moisture content has been measured using MB23 moisture analyser. The semi-batch Eirich EL1 type intensive mixer was used for mixing. The samples were homogeneously mixed with water at the fixed rotation speed (600 rpm) and time (20 min). Later, the samples were left to hydrate/cure in sealed and vacuumed containers at room temperature and were compacted on the following day using a hydraulic press into cylinders with diameter 20 ± 1 mm and height 20 ± 1 mm (Figure 3). Each batch of samples included minimum four cylindrical compacts and their average strength values are given in the results for each tested parameter.



Figure 3. Prepared cylindrical compacts of LFA (left), WA (middle), and OSA (right).

The physically bound water (moisture content) after overnight hydration (24 h) was measured to be $10 \pm 1\%$ for all samples before compaction, which was found to be a critical parameter for optimum compaction (without having any cracks due to dryness or erosion on the surfaces due to excessive water) based on previous experiences [20]. As press moulding of compacts was carried out with manual hand operated hydraulic press, serious attention has been given to the uniform preparation of samples. Two different compaction pressures (150 ± 10 and 300 ± 10 kgf/cm²) were applied to investigate the effect of compaction pressure. Carbonation experiments were performed in an automated carbonation unit (Figure 4) (stainless-steel 400 mL jacketed pressure vessel), consisting of apparatus controlling temperature (Circulator C-400) and monitoring CO₂ gas consumption (Buchi pressflow gas controller (bpc)).

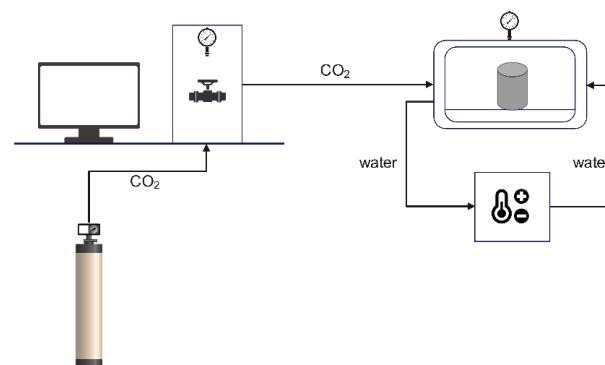


Figure 4. Scheme of the carbonation unit (including CO₂ gas cylinder, computer, pressure vessel).

Different sets of experimental conditions were applied, and parallel comparative tests were carried out to investigate the effects of different curing temperatures (25, 50, 75 °C), curing with typical flue gas CO₂ concentration (15% CO₂/6% O₂/N₂) compared to 100% CO₂, and different gas pressures (5, 10, and 15 bar) (see Table 3). To maintain stable CO₂ concentration during FG curing, the flushing and refilling steps were followed every 20 min. Furthermore, all tests were performed with the strategy of controlling the humidity using the potassium iodide saturated solution, which inhibits excessive humid conditions and maintains a RH between (61–68%) at different curing temperatures [34]. Density measurements were done with solid compacted cylinders.

Table 3. Experimental parameters to produce carbonated compacts.

Test Parameters		Curing CO ₂ %	Curing Gas Pressure	Curing Temperature	Compaction Pressure	Curing RH	Curing Time
Compaction pressure	150 kgf/cm ²	100% CO ₂	10 bar	25 °C	-	61–68%	2 h
	300 kgf/cm ²				-		
Gas Pressure	5 bar	100% CO ₂	-	25 °C	150 kgf/cm ²	61–68%	2 h
	10 bar						
	15 bar						
CO ₂ %	100% CO ₂	-	10 bar	25 °C	150 kgf/cm ²	61–68%	2 h
	16% CO ₂						
Temperature	25 °C	100% CO ₂	10 bar	-	150 kgf/cm ²	61–68%	2 h
	50 °C						
	75 °C						

3. Results

3.1. Variables Affecting CO₂ Uptake and Compressive Strength

3.1.1. Compaction Pressure and Mix Design

The forming compaction pressure of the FA in powder form prior to carbonation influences the physical properties of the compacted bodies and the mechanical properties of the resultant compacts. The porosity and permeability of the solid decrease when the compaction pressure is increased [35], which leads to a stronger structure and greater strength due to eliminated internal surface areas. Conversely, the lower gas permeability inhibits the penetration of the CO₂ passing through the inner surfaces of the compacted bodies. Thus, the efficiency of the accelerated carbonation process can be affected negatively due to the physical limitations of CO₂ permeability, diffusivity, and solubility, resulting in a lower amount of crystallized CaCO₃ formations and lower strength development. According to the obtained strength values of OSA, WA, and LFA there is a somewhat similar phenomenon as mentioned above. The results of compressive strength and CO₂ uptake of OSA, WA, and LFA together with mixed design compacts are presented in Figures 5 and 6.

The potential negative impact of increased compaction pressure on the CO₂ uptake of OSA compacts is negligible at the applied compaction pressure ranges. However, there are slight decreases on the CO₂ uptake level of WA and LFA compacts (Figure 5). The CO₂ uptake level of LFA with compaction pressure of 150 kg/cm² is 14.7% while samples with 300 kg/cm² compaction pressure is 11.9%, being the highest compared to the other ashes.

It is observed that a higher pressure of compaction (from 150 kg/cm² to 300 kg/cm²) leads to higher compressive strength in all prepared samples. The increase in compaction pressure results in an average compressive strength increase of 63% in OSA compacts, 71% in WA compacts, and 25% in LFA compacts (Figure 6). Compressive strength values of LFA compacts are 7.8 and 10.8 MPa for a compaction pressure of 150 and 300 kg/cm² showing the lowest values compared to other ashes. This is mainly due to LFA being composed of already formed CSH before compaction, which can reduce the compressive strength development.

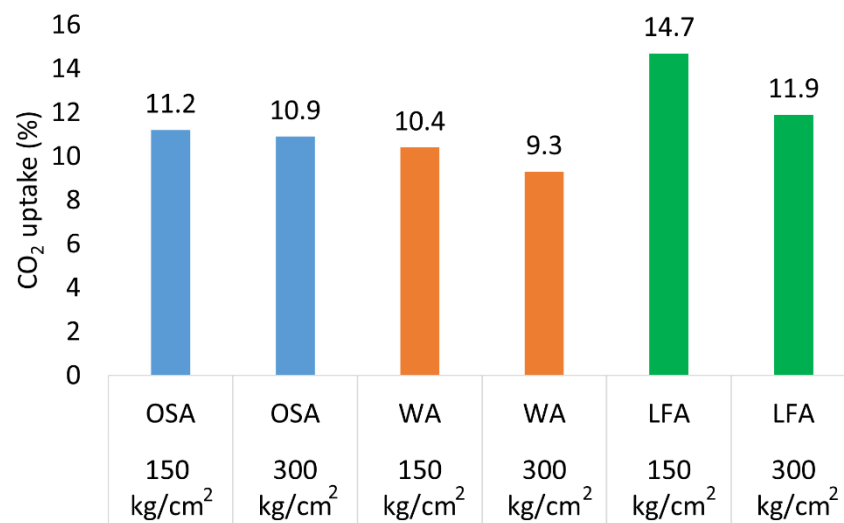


Figure 5. CO₂ uptake values at different compaction pressures for OSA, WA, and LFA (10 bar, 100% CO₂, 25 °C) (Average values obtained from min. 4 samples (std. deviation < 3%)).

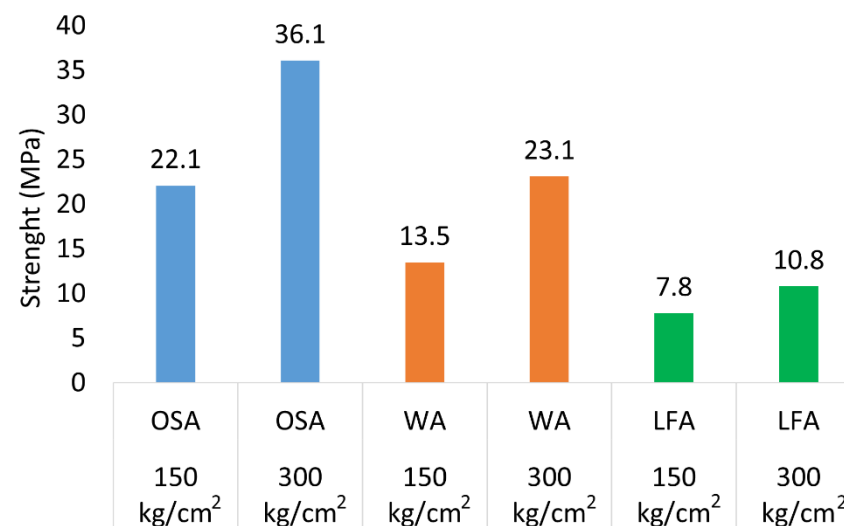


Figure 6. Compressive strength values at different compaction pressures for OSA, WA and LFA (10 bar, 100% CO₂, 25 °C) (Average values obtained from min. 4 samples (std. deviation < 2%)).

Two different types of mixed compacts were also designed; one containing 50% OSA/50% LFA (denoted by M1) and the other containing 50% WA/50% LFA (denoted by M2) (Figure 7). M1 compacts have an average compressive strength of 9.2 MPa while having a CO₂ uptake level of 13.1%. This indicates that LFA is slightly increasing the CO₂ uptake while reducing the compressive strength of the samples compared to 100% OSA compacts. M2 compacts have an average compressive strength of 10.4 MPa and CO₂ uptake level of 12.3%. A similar trend is observed with the strength and CO₂ uptake values of M2 compacts compared to 100% WA compacts. Both types of mixed designs exhibit more or less similar compressive strength and CO₂ uptake levels. LFA compacts exhibited overall lower density (1340 kg/m³) compared to OSA (1595 kg/m³) and WA (1830 kg/m³) compacts. Higher compaction pressure of 300 kg/cm² increased the density to 1470 kg/m³, which may show the potential usage of LFA for low density building material applications. Mixed designs demonstrate a median density based on the constituents. The M1 have an average density of 1380 kg/m³ and the M2 compacts have an average density of 1420 kg/m³ (see Table 4).

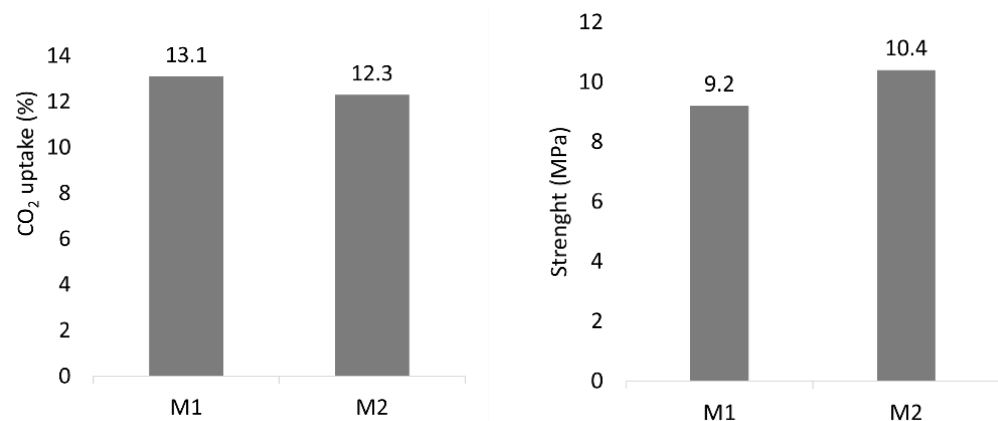


Figure 7. CO₂ uptake and compressive strength values of mixed design compacts (150 kgf/cm², 10 bar, 100% CO₂, 25 °C) (Average values obtained from min. 4 samples (std. deviation < 4%)).

Table 4. Density results of compacts (kg/m³).

	OSA	WA	LFA	M1	M2
150 kg/cm ²	1595	1830	1340	1380	1420
300 kg/cm ²	1720	1970	1470	1560	1690

3.1.2. Gas Pressure and CO₂ Concentration

CO₂ partial pressure and CO₂ concentration are factors affecting the rate of CO₂ uptake due to their effect on physisorption process at the interface between the solid and the gas reactant where the formation and growth of a solid product layer of CaCO₃ occurs [36]. The influence of the CO₂ gas pressure and CO₂ concentration was examined by evaluating CO₂ uptake levels and compressive strength of OSA and WA compacts. With the increase of gas pressures from 5 to 15 bar, the final CO₂ uptake levels as well as compressive strength increases in both the OSA and WA compacts. This could be explained with the improved gas penetration of CO₂ into the compact under high pressures, which favours the extent of carbonation reaction. At 5 bar, the CO₂ uptake percentage for OSA is 10.7% and for WA it is 8.2%. At 15 bar, the CO₂ uptake values are improved to 12.2% for OSA and 10.2% for WA (Figure 8). At 5 bar, the compressive strength value for OSA is 21.5 MPa and for WA it is 10.1 MPa. At 15 bar, the compressive strength values are increased to 34.5 MPa for OSA and 16.7 MPa for WA (Figure 9). For both samples, linear increasing dependency is observed at similar rates for CO₂ uptake and compressive strength measurements under increasing curing pressures (cured for 2 h).

It is also known that the CO₂ gas penetration into cementitious materials under high and low CO₂ concentration levels would be different, which affects the total CO₂ uptake levels. [37]. The CO₂ uptake value for OSA is 10.8% and for WA it is 9.4% at the curing with 100% CO₂ concentration. The CO₂ uptake values are decreased to 7.6% for OSA and 7.9% for WA (Figure 10) at the curing with FG (16% CO₂). The compressive strength of samples cured in 100% CO₂ are higher than the samples cured in FG, which is in line with less CO₂ uptakes. Due to the higher content of Ca-Mg silicates, which participate in hydraulic or pozzolanic reactions in OSA compacts, the compressive strength values were higher than WA compacts. At longer curing periods, CO₂ uptake values of FG curing can reach the same level as 100% CO₂ curing.

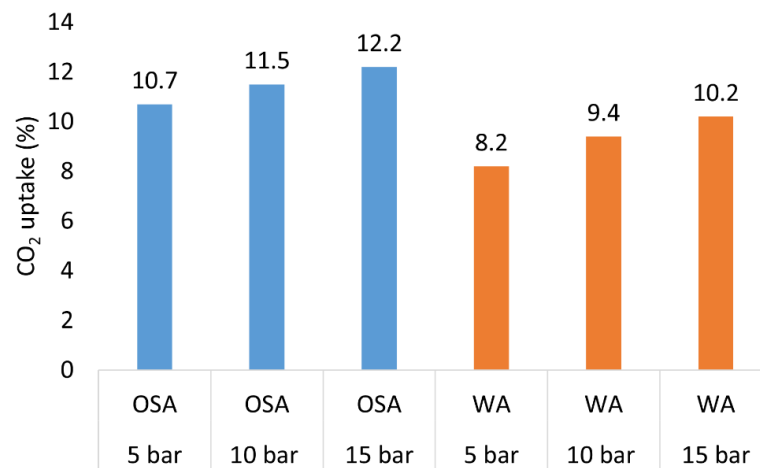


Figure 8. CO₂ uptake values at different curing pressures (100% CO₂, 25 °C, 150 kg/cm²) (Average values obtained from min. 4 samples (std. deviation < 3%)).

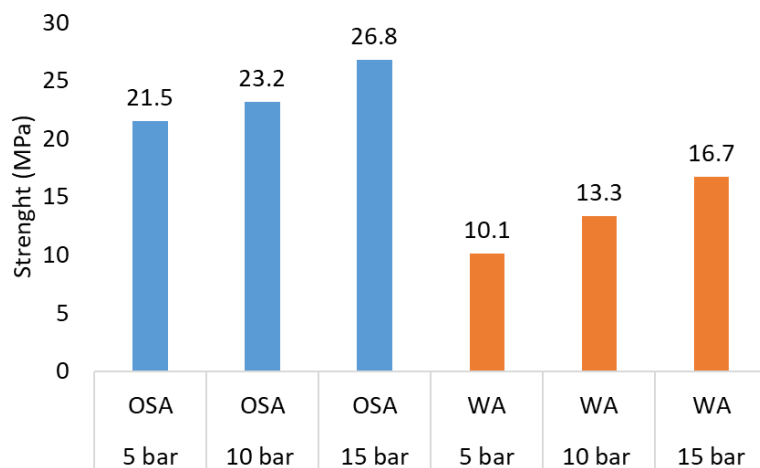


Figure 9. Compressive strength values at different curing pressures (100% CO₂, 25 °C, 150 kg/cm²) (Average values obtained from min. 4 samples (std. deviation < 3%)).



Figure 10. CO₂ uptake (left) and compressive strength (right) values at different CO₂ concentrations (10 bar, 25 °C, 150 kgf/cm²) (Average values obtained from min. 4 samples (std. deviation < 3%)).

3.1.3. Temperature

It is noted in previous studies that the temperature during carbonation influences the dissolution rate of constituents, the solubility of CO₂ and the morphology and mineralogy of the carbonates [23]. An increase in process temperature simultaneously increases the

rates of all the chemical processes but reduces the CO₂-solubility in water and thus CO₂-availability [38]. The influence of temperature was examined by evaluating CO₂ uptake levels (Figure 11) and compressive strength (Figure 12). In both samples, the CO₂ uptake levels are elevated at higher temperatures; however, the same is not true for strength development. This indicates that a higher CO₂ uptake does not always validate higher strength development. A higher carbonation degree at high temperature can cause the double-chain silicate anion structure of CSH to decompose and consequently slow the compressive strength gain [39]. It is known that with increased carbonation, the micro-mechanical property of CSH is weakened [40]. For OSA, the highest compressive strength value (24.8 MPa) is attained at 50 °C. For WA, the highest compressive strength (14.7 MPa) is attained at 25 °C. For both samples, the lowest strength value is attained at the highest temperature. Reduction in compressive strength at higher temperatures in both samples can also be explained by the initial fast CO₂ uptake, causing weaker carbonate crystals in compacts. The temperature effect on the stability of carbonates is further discussed in the thermal analysis section.

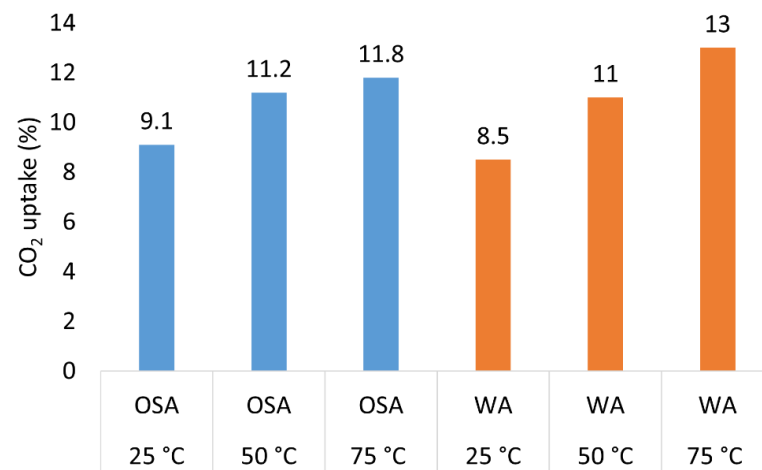


Figure 11. CO₂ uptake values at different temperatures (10 bar, 100% CO₂, 150 kgf/cm²) (Average values obtained from min. 4 samples (std. deviation < 3%)).

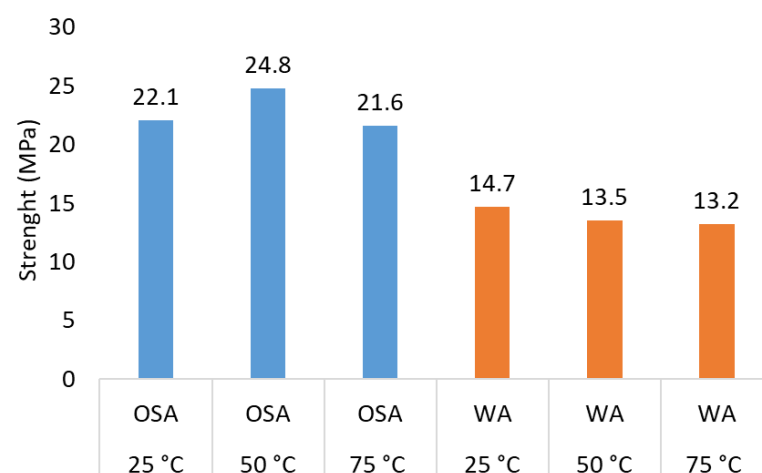


Figure 12. Compressive strength values at different temperatures (10 bar, 100% CO₂, 150 kgf/cm²) (Average values obtained from min. 4 samples (std. deviation < 3%)).

3.2. Thermal Analysis

Based on the TGA/DTG curves of uncarbonated samples, there are three major mass loss steps which occur: First, related to water loss due to evaporation and later dehydration of crystalline and amorphous components i.e., ettringite (up to 200 °C); second, dehydration

of $\text{Ca}(\text{OH})_2$ (up to 500 °C) (Equation (1)); and third, CO_2 loss due to decomposition of CaCO_3 (between 550–900 °C) (Equation (2)) (Figures 13 and 14).

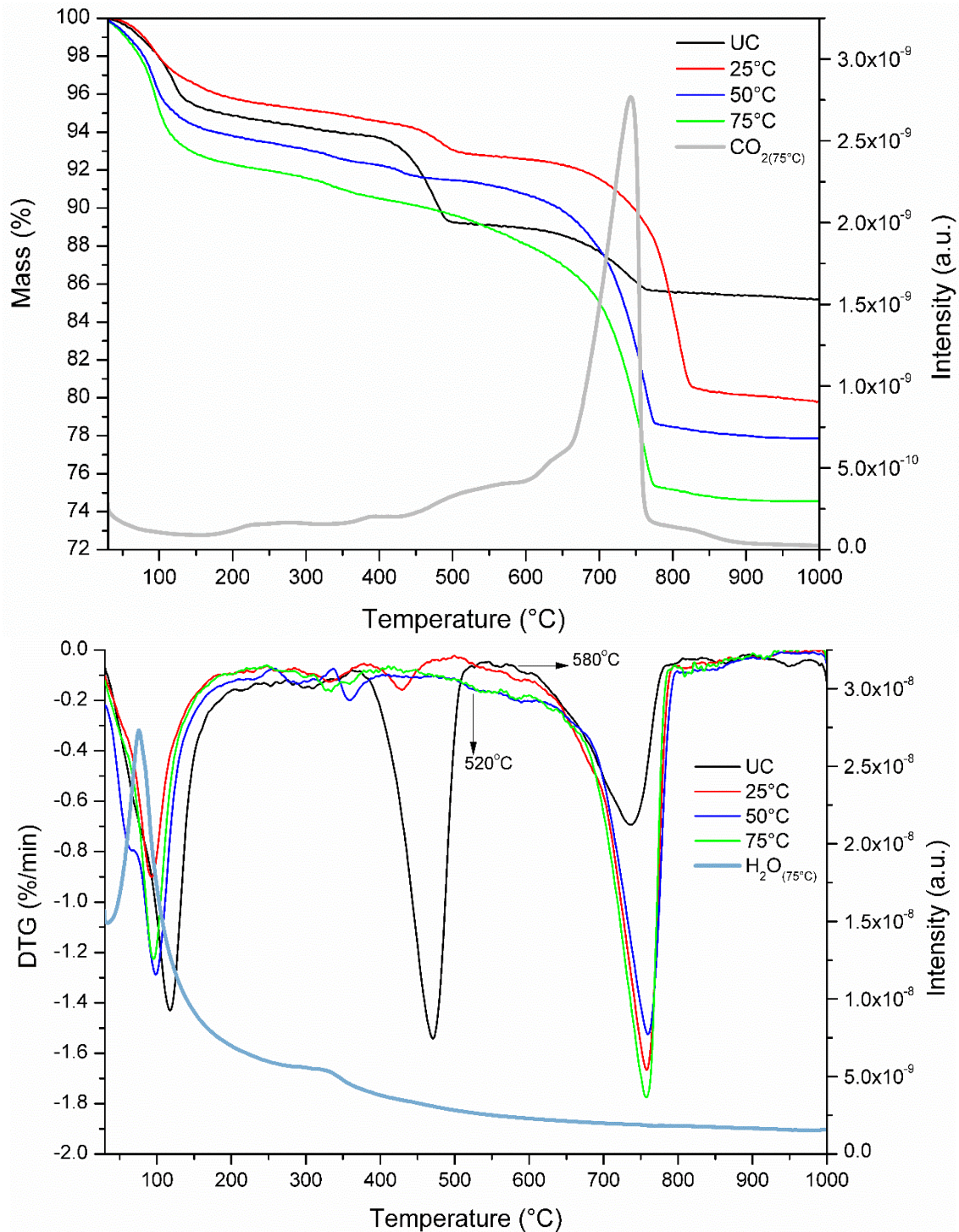
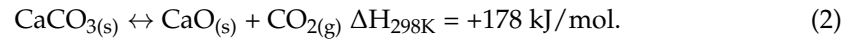
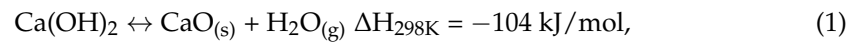


Figure 13. TGA and DTG with MS (75 °C) of OSA compacts that are uncarbonated (UC) and cured at 25 °C, 50 °C, and 75 °C.

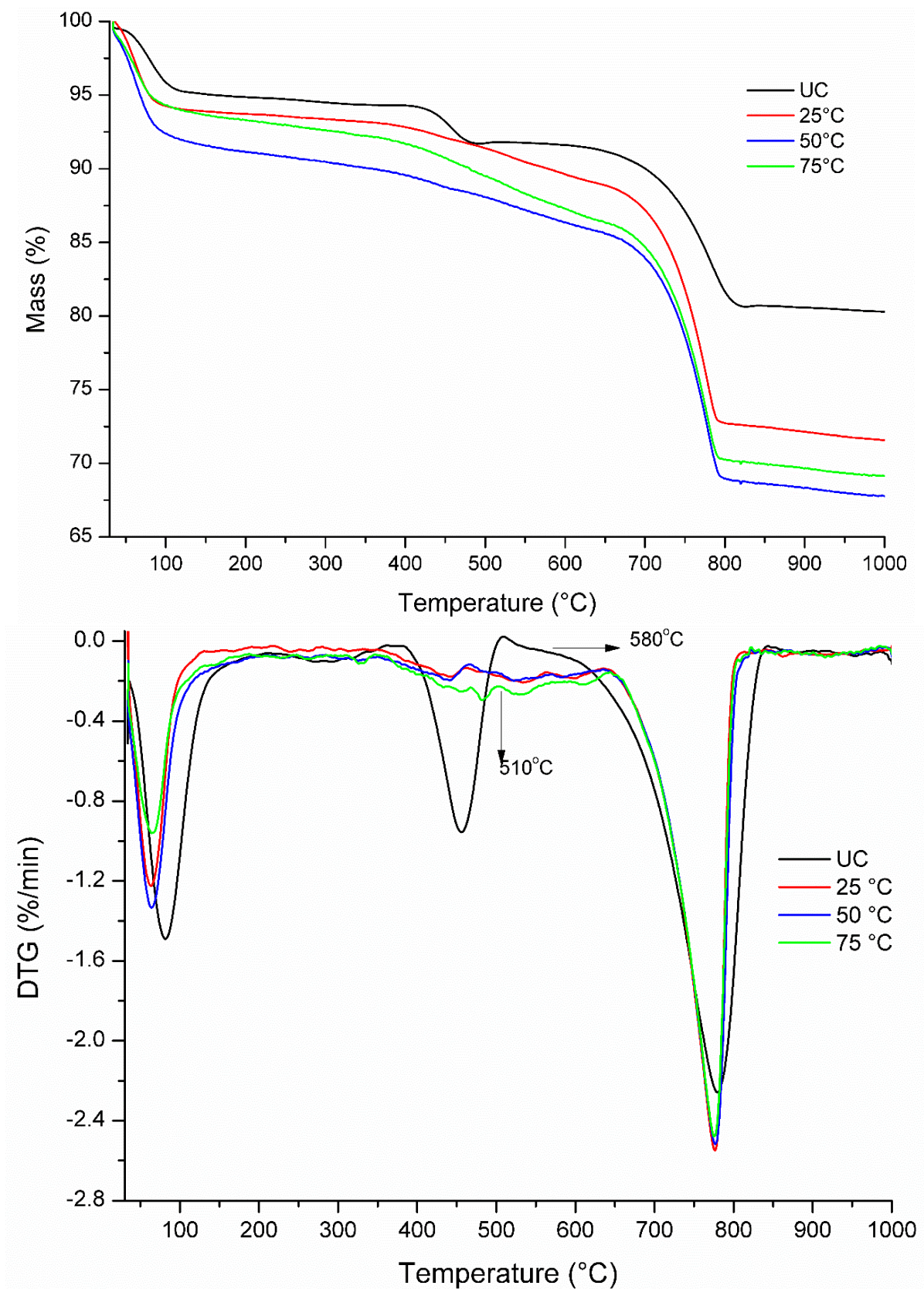
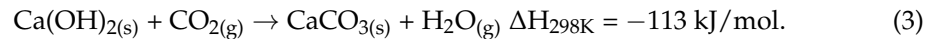


Figure 14. TGA and DTG of WA compacts that are uncarbonated (UC) and cured at 25 °C, 50 °C, and 75 °C.

There are mainly two mass loss step (water evaporation and CO₂ release from CaCO₃) for carbonated samples as the mass loss related to water from Ca(OH)₂ is not significant due to the carbonation of Ca(OH)₂ (Equation (3)), except for OSA carbonated at 25 °C. MS curves of OSA compacts cured at 75 °C are supporting the outcomes of the TGA curves (Figure 13).



As can be seen from the third mass loss step of uncarbonated samples, both ashes already include CaCO₃ in their initial forms (before hydration and carbonation). Therefore, the net CO₂ uptake is calculated by subtracting the initial (uncarbonated) mineral CO₂ related mass loss from the total CO₂ related mass loss of carbonated samples. Samples cured at 25 °C had a CO₂ uptake of 9.1 and 8.5%, respectively, for OSA and WA.

In connection with previous section, the effect of curing temperature can also be followed by both TGA/DTG curves, showing that there is clear increase in CO₂ uptake values with increased curing temperatures of 25, 50, and 75 °C. Besides, the thermal stability of the newly formed CaCO₃ can also be characterized by looking at the TG/DTG curves. The onset temperatures (for OSA, 520 °C for curing temperatures of 25, 50 and 75 °C and 580 °C for initial sample. For WA, 510 °C for curing temperatures of 25, 50 and 75 °C and 580 °C for initial sample (Figure 14)) of the DTG curves representing the initial stage of decomposition CaCO₃ of carbonated samples are slightly lower than the detected onset temperatures of uncarbonated samples. Several authors have also presented similar findings of low thermal decomposition temperatures for CaCO₃ in case of occurrence in the not well crystalline form of calcite [41]. This may show different thermal stability of the formation of new CaCO₃ phases at above room temperatures within the applied curing conditions. This can also be attributed to poor transformation of amorphous CaCO₃ into calcite, which generally has more stable formations at room temperature [42]. However, it is also known that the thermal stability of amorphous calcium carbonate could eventually increase and spontaneously crystallize.

3.3. Kinetic Analysis

The experimental real time gas monitoring results of both OSA and WA compact carbonation are shown in Figures 15 and 16, where the CO₂ consumption kinetics are plotted at different temperatures. The carbonation reaction in OSA and WA compact are both fast at the initial stage, which can be explained by the available open porous surfaces and sufficient amount of physically bound water in the open pore structures of the specimens providing a fast start of carbonation. After this stage, a stage with a slower reaction rate takes place due to the diffusion limitation through the product layer, as carbonation proceeds from the outer surface into the internal spaces. Besides, initial fast exothermic carbonation reaction also influences the particle temperatures, which can accelerate the evaporation of the physically bound water. This would cause a restriction on the diffusion of CO₂ and carbonic acid formation. Although there is no clear temperature dependency at the initial stage of the carbonation reaction, there is a positive effect of increasing temperature on CO₂ uptake especially in the diffusion-controlled stage of OSA. The CO₂ consumption trend in terms of the carbonation rate is slightly different in WA compared to OSA and varies in different temperatures. The positive effect of increasing temperature on the rate growth of WA carbonation is more apparent, pointing out more kinetic controlled reaction phenomena, already at the early carbonation stage. The increase in temperature elongates the time of the fast carbonation period, provided that the WA reacts for a longer time, before the process reaches a more diffusion-controlled stage. The CO₂ uptake values obtained from the gas monitoring results support the total CO₂ uptake values detected in thermal analysis. The final conversion values after 2 h of curing are for OSA 0.57–0.63 and for WA 0.42–0.61. The extrapolation of graphs show that full conversion can be achieved in 12–14 h for OSA and 13–16 h for WA.

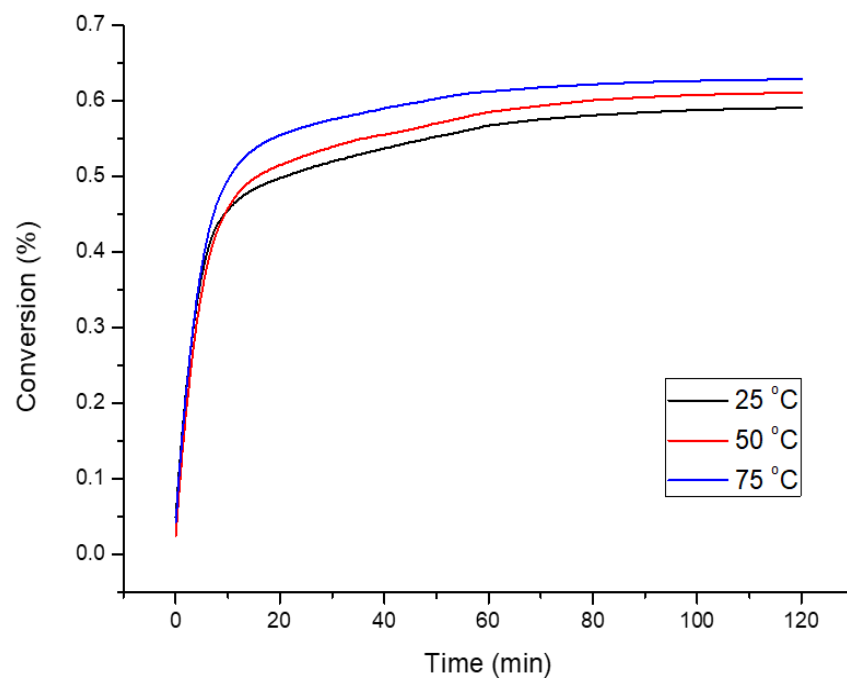


Figure 15. Gas consumption curves of OSA compacts cured at 25 °C, 50 °C, and 75 °C.

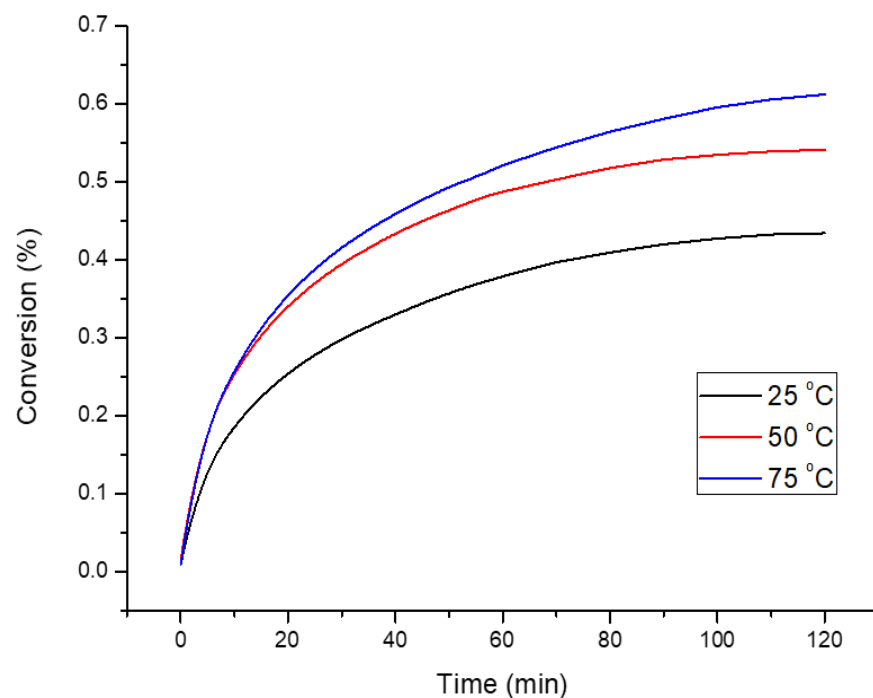


Figure 16. Gas consumption curves of WA compacts cured at 25 °C, 50 °C, and 75 °C.

By using real time gas monitoring results obtained at three different temperatures, the reaction kinetics of the carbonation conversion were tested by different diffusion-controlled reaction-order models [43]. It is known that carbonation of Ca-Mg silicates is less reactive at alkali conditions compared to $\text{Ca}(\text{OH})_2$, where pH values should drop to 10 according to equilibrium calculations [6]. The obtained pH values could be considered to understand whether all Ca and Mg bearing phases are participating into carbonation reactions (see Appendix A). As the obtained pH values are around 11.5, the participation of Ca-Mg silicates into carbonation reaction should be negligible. Therefore, the amount of total CO_2 that can bound during carbonation is calculated according to most reactive available

phases of the ashes, which are CaO and Ca(OH)₂ without including Ca-Mg silicates. The quantitative XRD analysis (see Table 2) results of initial OSA and WA were used as the basis for the calculation with Equation (4) given below. In order to estimate and compare the CO₂ binding ability of different samples, CO_{2max}, the maximal possible CO₂ uptake capacity of the samples was calculated on the basis of the Ca(OH)₂ (taking into account its CaO as free CaO) and free CaO content of initial sample.

$$\text{CO}_{2\max}(\%) = \frac{\text{CaO}(\%)}{\frac{\text{MCaO}}{\text{MCO}_2}} + \frac{\text{Ca(OH)}_2(\%)}{\frac{\text{MCa(OH)}_2}{\text{MCO}_2}}. \quad (4)$$

Previous studies have shown that carbonation kinetics of industrial alkaline solid wastes [44,45] can be sufficiently demonstrated by two solid-state kinetic models, which were combined into Equation (5) [46]:

$$1 - (1 - \alpha)^{1/3} = kt, \quad (5)$$

where k is the rate constant, t is the reaction time, n is a (parametrizable) index of the rate determining step, and α is the conversion degree (carbonation turnover, $\alpha = 1$ for full carbonation) according to Equation (6).

$$\alpha = m_0 - m_t / m_0 - m_f, \quad (6)$$

where, m_0 is the initial weight, m_t is the weight at time t , and m_f is the final weight.

By adapting the exponent n in Equation (5), two kinetic models can be defined. For $n = 1$, Equation (5) represents a purely phase-boundary controlled reaction that applies to the initial stages of carbonation. For $n = 2$, Equation (5) applies to a diffusion-limited reaction (Jander equation), where the rate-limiting step is diffusion through the growing layer of precipitated CaCO₃. The conformity between experimental data and the kinetic model was expressed by the correlation coefficients (R^2).

The Arrhenius equation is presented below.

$$k = Ae^{-(E_a/RT)}, \quad (7)$$

where k is the rate constant, A is the pre-exponential (frequency) factor, e is Euler's number, E_a is the activation energy, T is absolute temperature, and R is the gas constant. The activation energy can be determined from the slope of the transformed equation $\ln(k) = \ln(A) - E_a/RT$ (8) with the linear fitting of $\ln(k)$ and $1/T$ (See Appendix B). The activation energy (E_a) for OSA has been calculated as 3.55 kJ/mol and for WA as 17.06 kJ/mol. The activation energy values exhibited in literature for CaO and Ca(OH)₂ carbonation reactions are in line with the calculated values in this work [47].

Figure 17 shows the converted experimental data of the carbonation tests (i.e., $\ln(1 - (1 - \alpha)^{1/3})$ vs. $\ln(t)$). A relatively high R^2 value indicates that the model adequately represents the kinetics of carbonation. The values of Equation (5) to the converted data suggest that the reaction is phase-boundary controlled during the initial stages of accelerated carbonation for OSA ($\ln(t) < 2.5$) and WA ($\ln(t) < 2.9$) samples. After the change in reaction rate, carbonation becomes controlled by diffusion through the product-layer. The transition between the two kinetic models is illustrated by the change of the slope for the plot of $\ln(1 - (1 - \alpha)^{1/3})$ vs. $\ln(t)$. For WA reaction conditions, the change in slope seems to be less pronounced and later than OSA, which can be related to higher SSA of WA delaying the beginning of the diffusion phase, which is in line with the CO₂ monitoring graphs (Figures 14 and 15). This indicates that rate limitations by diffusion through a growing layer of precipitated CaCO₃ are less important when the solid is in motion (exposure of internal surfaces), corroborating the higher CO₂-uptake.

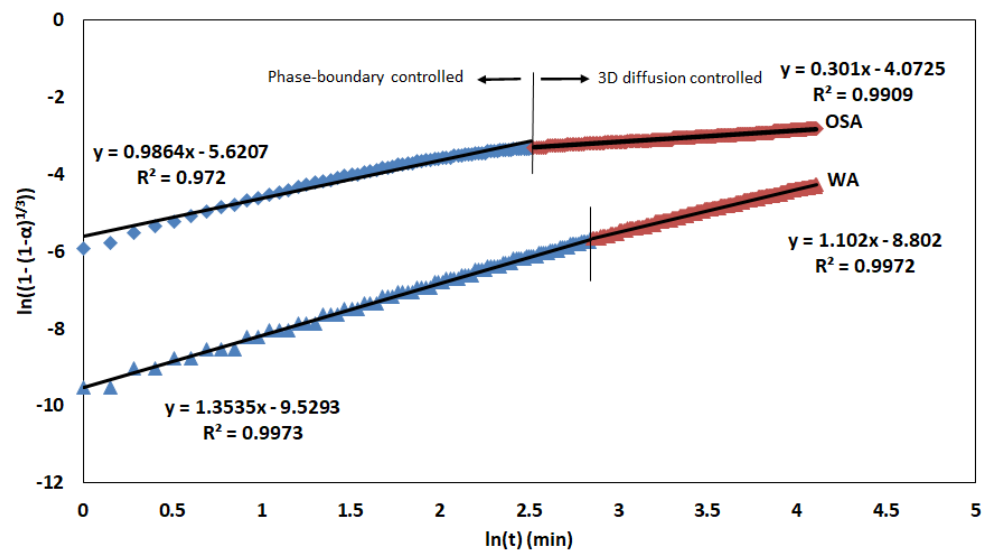


Figure 17. Evaluation of carbonation kinetics: $\ln(1 - (1 - \alpha)^{1/3})$ versus $\ln(t)$ for OSA and WA carbonation (R^2 = correlation coefficient).

3.4. Microstructural and Mineralogical Changes

3.4.1. XRD Analysis

XRD analysis was performed to confirm the products of carbonation and to identify what phases were consumed in the reaction. Evidence suggested that Portlandite was consumed almost completely, while calcite was the primary product. The XRD patterns of the hydrated samples in Figures 18 and 19 show evidence of some pre-existing carbonates present as calcite in the hydrated ashes, while the sample patterns included clear portlandite peaks for both OSA and WA. A good match was found in comparing the XRD pattern of the carbonated compacts to the XRD pattern of natural calcite, which confirmed that the major carbonation product was calcite. The carbonated samples showed new and more intense XRD peaks corresponding to calcite. The trace amount of Aragonite was detected with minimal intensities, which are not displayed here. Pre-existing Quartz peaks were identified in both OSA (higher intensity) and WA. CSH peaks were identified in both hydrated and carbonated samples, which indicates that CS were hydrated by the hydration process. Anhydrite and Ettringite were present in the OSA samples only.

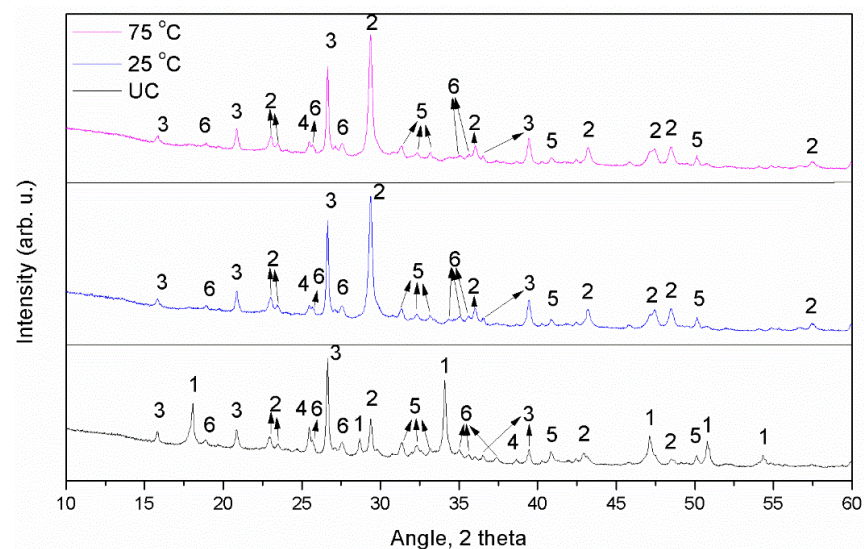


Figure 18. XRD patterns of OSA hydrated uncarbonated (UC), cured at 25 °C and 75 °C: 1—Portlandite; 2—Calcite; 3—Quartz; 4—Anhydrite; 5—CSH; 6—Ettringite.

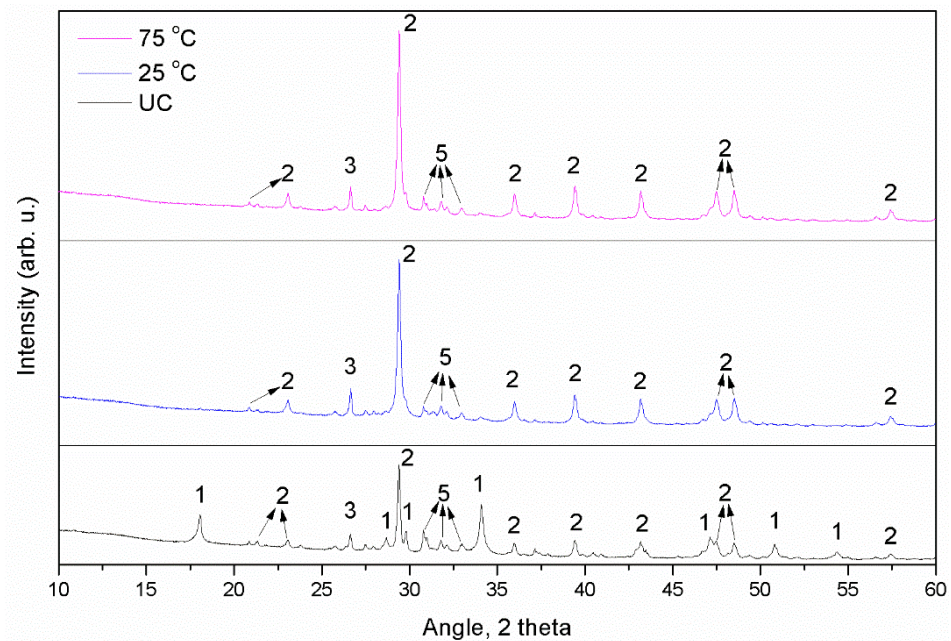


Figure 19. XRD patterns of WA hydrated uncarbonated (UC), cured at 25 °C and 75 °C: 1—Portlandite; 2—Calcite; 3—Quartz; 5—CSH.

3.4.2. SEM Analysis

Figure 20a shows the microstructure of an area near the surface of the hydrated OSA compact. Figure 20b shows the 5000× magnified surface of compact cured at 25 °C. Although the particles are not definitively separate and the hydrated products seem to be fused together, the hexagonal portlandite lamellar appears to be covered by irregular, flaky, and grainy products with dimensions in the order of 1 μm. The porous surface structure of the hydrated OSA compact changes after carbonation and becomes more compact. No visible portlandite crystals are identified in the carbonated compacts, which agrees with the near total conversion suggested by the XRD data. The carbonated products have fused into a coating that makes it difficult to discern the shape or location of the original OSA particles. It has been suggested [48] that the carbonation reaction products end up becoming intermixed into calcium silicate hydrate, such that it is unable to identify distinct carbonation product morphologies with SEM analyses. Nevertheless, the gel and the carbonation products have filled the spaces between the particles or even fused them together. The effect of fast carbonation in higher temperatures is observed as micro crack formations, which can explain the lower strength values attained at the highest temperature (75 °C) (Figure 21). Similarly, the microstructure of the hydrated WA specimen, as seen in Figure 22a, displays distinct morphological evidence of a more open structure near the surface of the hydrated WA compact. Figure 22b shows more compact structure of the WA compact cured at 25 °C, covered with globular formations. Some acicular or flaky products can be seen and were identified as calcium carbonates. Agglomeration of calcium silicate hydrate particles forming gel like structures surrounding the calcium carbonates can be observed. In carbonated compacts, no portlandite crystals are identified, which agrees with the near total conversion suggested by the XRD data.

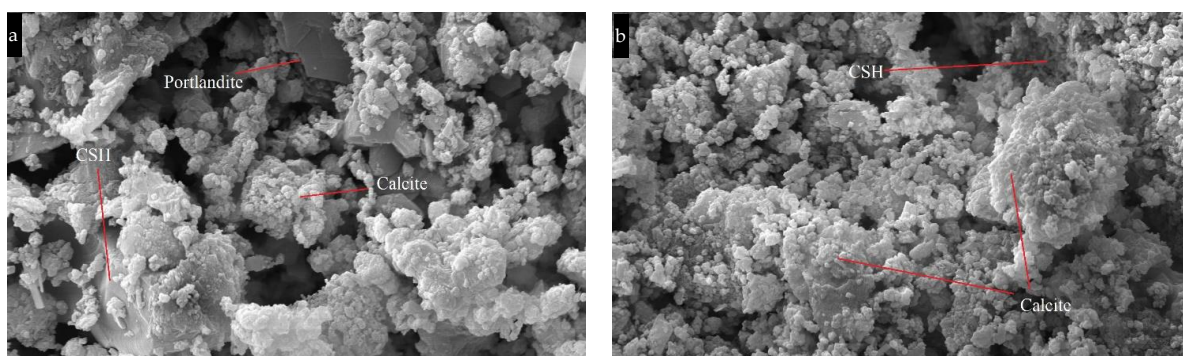


Figure 20. SEM images of OSA compacts 5000× magnified ((a) hydrated, (b) cured at 25 °C, 10 bar, 100% CO₂, 150 kgf/cm²).

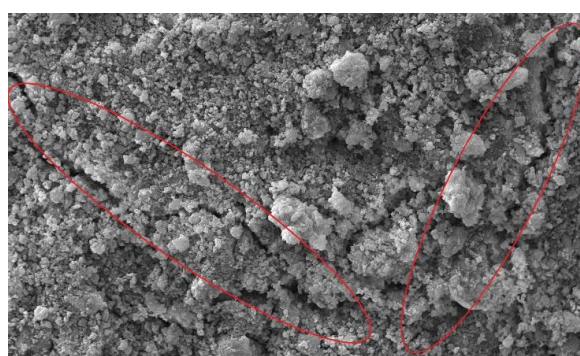


Figure 21. SEM image of OSA compact 2000× magnified exhibiting microcracks (cured at 75 °C, 10 bar, 100% CO₂, 150 kgf/cm²).

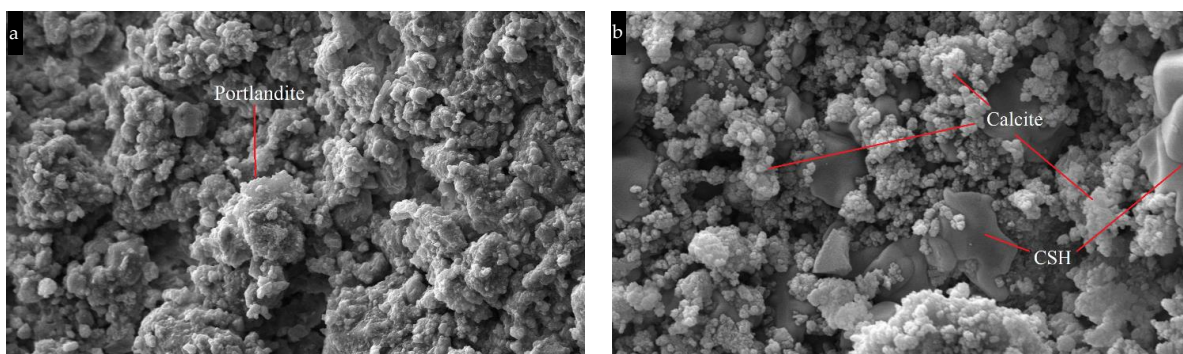


Figure 22. SEM images of WA compacts 5000× magnified ((a) hydrated, (b) cured at 25 °C, 10 bar, 100% CO₂, 150 kgf/cm²).

3.5. Current Results in the Context of Sustainable Building Materials

The construction materials sector needs to become more diversified and sustainable, as well as safe and performant, in order to meet the stringent environmental and technical demands [49–51]. Furthermore, based on the type and availability of secondary raw materials from various industrial units, the manufacturing of new construction materials should be customized to local resources.

There are a variety of commercial technologies that combine CO₂ with solid waste streams due to the growing interest in waste mineralization as a feasible carbon capture and utilization technology. For instance, an accelerated carbonation technique was developed by Carbon8 Systems Ltd. (Gillingham, UK) for the remediation of industrial wastes and contaminated soils to produce construction products [52]. Additionally, Carbicrete (Montreal, Canada) uses a mineral carbonation method to create a concrete manufactured

from mainly steel slags and CO₂ (8% from flue gas) with a compressive strength 50% higher than ordinary concrete [53]. In addition, Carbstone Innovation (Genk, Belgium) uses CO₂ to cure slags from electric arc furnaces and basic oxygen furnaces for use as building material [54]. Similar to the commercialized technologies above, when the results of this study are considered for a specific target product, the process can be improved and optimized in line with the associated standards.

Compressive strength of 10–36 MPa and CO₂ uptake of 11–15% mass was achieved by mineral carbonation. These findings show that there is a room for improvement and potential for future applications such as kerbstone paver and paving blocks. The findings exhibited better performance of compressive strength compared to previous explorations of cementitious properties of similar FAs [20]. Telesca et al. [55,56] studied coal FA as a raw material to produce ettringite-based construction materials and discovered that it has the potential to be used in this method. They obtained a maximum compressive strength of around 6 MPa, which was achieved after 16 h of curing. Self-cementitious characteristics and pozzolanic reactivity of FA were examined by Li et al. [57]. They achieved a compressive strength of 11.4 MPa without chemical modifiers after 28 days, and 22.4 MPa with chemical modifiers and particle size distribution optimization. Ohenoja et al. [58] discovered that compressive strength was dependent on the selectively soluble calcium, aluminium, silicate, and sulphate content. Tests including different FAs have achieved a compressive strength of up to 6 MPa after 28 days.

4. Conclusions

This study analyses the performance of compacts produced from locally sourced distinct FAs such as OSA, WA, and LFA, in terms of CO₂ uptake and compressive strength under numerous process conditions (i.e., 25–75 °C, 5–15 bar, 15–100% CO₂, and compaction pressures of 150 and 300 kgf/cm²).

Among the two main samples, OSA compacts exhibited 10–12 wt% CO₂ uptake with a compressive strength of 16–36 MPa, whereas WA compacts show a wider range of 8–13 wt% CO₂ uptake with a compressive strength of 10–16 MPa. Preliminary findings of LFA indicate that there is a future potential for applications of lightweight building materials by utilizing previously deposited combustion residues, binding ~15 wt% CO₂.

Changes in the curing conditions have a direct effect on the CO₂ uptake levels and related strength development;

- Increase in gas pressure and CO₂ concentration exhibited positive correlation with the CO₂ uptake and compressive strength values;
- Compaction pressure as a pre-processing parameter is mainly related to compressive strength. However, due to its physical effect on diffusivity, the compaction pressure increase showed an increase in strength while limiting CO₂ penetration in a small amount, causing less CO₂ uptake;
- Despite higher carbonation degrees at elevated curing temperatures, the compressive strength did not increase accordingly. High temperatures can increase the risks of micro cracks and change the micro-mechanical property of CSH, which in turn weakens the compressive strength;
- Additionally, at high temperatures, due to the reduction of liquid water in compacts, uneven and fast formation of particulates (amorphous formations of calcite polymorphs) on the surfaces of mainly Ca(OH)₂ can appear, yet such determination is rather complex for short curing times (2 h);
- SEM and XRD analysis further proved that Calcite was the dominant phase after carbonation and portlandite was almost completely consumed;
- Reaction mechanism corresponds to 3D-diffusion-controlled reaction order model for both OSA and WA. CO₂ diffusion through the product layer was estimated to be the rate-controlling step and surface passivation was clearer for OSA, except for WA, due to the short curing time. Calculated apparent activation energies are given for OSA as 3.55 kJ/mol and for WA as 17.06 kJ/mol.

The prospective result of this study enables greater insight into the CO₂ curing processes of ashes, which can be transferred to the industrial building material applications for tailoring of the locally available Estonian ash as well as similar ash elsewhere.

Author Contributions: Conceptualization, M.C.U.; methodology, M.C.U. and C.R.Y.; software, M.C.U.; validation, M.C.U., C.R.Y. and M.U.; formal analysis, M.C.U.; investigation, M.C.U.; resources, M.C.U. and A.G.; data curation, M.C.U.; writing—original draft preparation, M.C.U.; writing—review and editing, M.C.U., C.R.Y. and T.H.; visualization, M.C.U.; supervision, C.R.Y. and M.U.; project administration, A.T.; funding acquisition, A.T. All authors have read and agreed to the published version of the manuscript.

Funding: This research is funded by the CLEANKER project which has received funding from the European Union’s Horizon 2020 Framework Program under Grant Agreement No. 764816 and the Government of China (National Natural Science Foundation of China) under contract No. 91434124 and No. 51376105. This work is also partially supported by ASTRA “TUT Institutional Development Program for 2016–2022” Graduate School of Functional Materials and Technologies and the Estonian ministry of Education and Research (IUT33-19).

Institutional Review Board Statement: Not applicable.

Informed Consent Statement: Not applicable.

Data Availability Statement: Not applicable.

Acknowledgments: This work was carried out as part of a Ph.D. project supported by the Estonian Ministry of Education and Research (IUT33-19). This work has been partially supported by ASTRA “TUT Institutional Development Program for 2016–2022” Graduate school of Functional Materials and Technologies. The help of Mart Viljus (SEM images) is gratefully acknowledged.

Conflicts of Interest: The authors declare no conflict of interest. The funders had no role in the design of the study; in the collection, analyses, or interpretation of data; in the writing of the manuscript, or in the decision to publish the results.

Appendix A

Table A1. pH measurements of compacts (UC: Uncarbonated, 25 °C: Carbonated at 25 °C, 75 °C: Carbonated at 75 °C).

	OSA			WA		
	UC	25 °C	75 °C	UC	25 °C	75 °C
pH	12.5	11.5	11.4	12.7	12.1	11.4

Appendix B

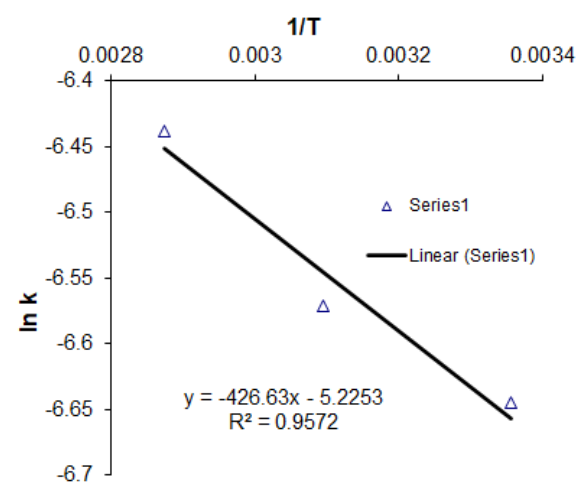
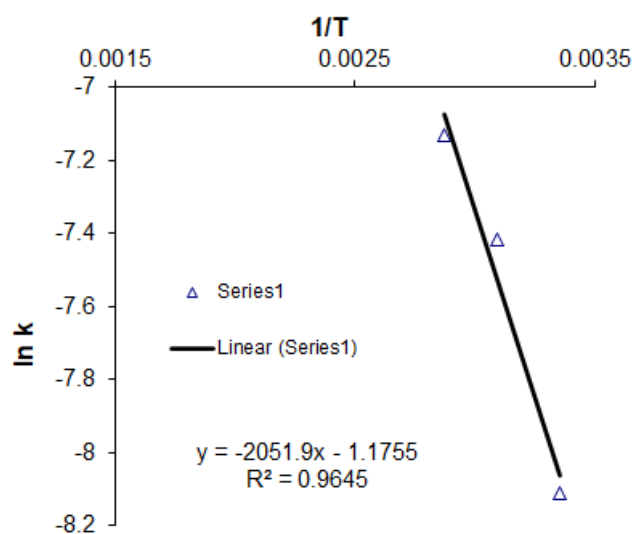


Figure A1. Arrhenius chart for OSA compacts.

Table A2. Reaction parameters for OSA compacts.

T, K	1/T	k	ln k
298	0.003355705	1.3×10^{-3}	-6.64539
323	0.003095975	1.4×10^{-3}	-6.57128
348	0.002873563	1.60×10^{-3}	-6.43775
Slope:	-426.63	Intercept:	-5.2253
E_A	3.54700182	kJ/mol	
A	0.005378746	min^{-1}	

**Figure A2.** Arrhenius chart for WA compacts.**Table A3.** * Reaction parameters for WA compacts.

T, K	1/T	k	ln k
298	0.003355705	3.0×10^{-4}	-8.11173
323	0.003095975	6.0×10^{-4}	-7.41858
348	0.002873563	8.00×10^{-4}	-7.1309
Slope:	-2051.9	Intercept:	-1.1755
E_A	17.0594966	kJ/mol	
A	0.308664609	min^{-1}	

* (T: Temperature (K), k: Rate constant, E_A : Activation Energy, A: Pre-exponential factor).

References

- Torgal, F.P.; Shi, C.; Angel, S.P. Accelerated carbon dioxide sequestration. In *Carbon Dioxide Sequestration in Cementitious Construction Materials*; Woodhead Publishing: Sawston, UK, 2018; pp. 81–101.
- IEA Cement Tracking Report, November 2021. Available online: <https://www.iea.org/reports/cement> (accessed on 4 December 2021).
- Scrivener, K.L.; John, V.M.; Gartner, E.M. Eco-efficient cements: Potential economically viable solutions for a low- CO_2 cement-based Materials Industry. *Cem. Concr. Res.* **2018**, *114*, 2–26. [CrossRef]
- HeidelbergCement AG. HeidelbergCement to Install the World's First Full-Scale CCS Facility in a Cement Plant. Available online: <https://www.heidelbergcement.com/en/pr-15-12-2020> (accessed on 15 December 2020).
- Yi, H.; Xu, G.; Cheng, H.; Wang, J.; Wan, Y.; Chen, H. An overview of utilization of steel slag. *Procedia Environ. Sci.* **2012**, *16*, 791–801. [CrossRef]
- Von Greve-Dierfeld, S.; Lothenbach, B.; Vollpracht, A.; Wu, B.; Huet, B.; Andrade, C.; Medina, C.; Thiel, C.; Gruyaert, E.; Vanoutrive, H.; et al. Understanding the carbonation of concrete with supplementary cementitious materials: A critical review by RILEM TC 281-CCC. *Mater. Struct.* **2020**, *53*, 136. [CrossRef]

7. Hemalatha, T.; Ramaswamy, A. A review on fly ash characteristics—Towards promoting high volume utilization in developing sustainable concrete. *J. Clean. Prod.* **2017**, *147*, 546–559. [CrossRef]
8. Ramezani-pour, A.A. *Cement Replacement Materials*; Springer Geochemistry/Mineralogy: New York, NY, USA, 2014; pp. 70–74. ISBN 9783642367205.
9. Moon, E.J.; Choi, Y.C. Carbon dioxide fixation via accelerated carbonation of cement-based materials: Potential for construction materials applications. *Constr. Build. Mater.* **2019**, *199*, 676–687. [CrossRef]
10. Mo, L.; Zhang, F.; Deng, M.; Jin, F.; Al-Tabbaa, A.; Wang, A. Accelerated carbonation and performance of concrete made with steel slag as binding materials and aggregates. *Cem. Concr. Compos.* **2017**, *83*, 138–145. [CrossRef]
11. Guo, M.Z.; Tu, Z.; Poon, C.S.; Shi, C. Improvement of properties of architectural mortars prepared with 100% recycled glass by CO₂ curing. *Constr. Build. Mater.* **2018**, *179*, 138–150. [CrossRef]
12. Wei, Z.; Wang, B.; Falzone, G.; La Plante, E.C.; Okoronkwo, M.U.; She, Z.; Oey, T.; Balonis, M.; Neithalath, N.; Pilon, L.; et al. Clinkering-free cementation by fly ash carbonation. *J. CO₂ Util.* **2018**, *23*, 117–127. [CrossRef]
13. Woodall, C.M.; McQueen, N.; Pilorgé, H.; Wilcox, J. Utilization of mineral carbonation products: Current state and potential. *Greenh. Gas. Sci. Technol.* **2019**, *9*, 1096–1113. [CrossRef]
14. Chang, R.; Kim, S.; Lee, S.; Choi, S.; Kim, M.; Park, Y. Calcium carbonate precipitation for CO₂ storage and utilization: A review of the carbonate crystallization and polymorphism. *Front. Energy Res.* **2017**, *5*, 17. [CrossRef]
15. Uibu, M.; Kuusik, R.; Andreas, L.; Kirsimäe, K. The CO₂ binding by Ca-Mg-silicates in direct aqueous carbonation of oil shale ash and steel slag. *Energy Procedia* **2011**, *4*, 925–932. [CrossRef]
16. Bobicki, E.R.; Liu, Q.; Xu, Z.; Zeng, H. Carbon capture and storage using alkaline industrial wastes. *Prog. Energy Combust. Sci.* **2012**, *38*, 302–320. [CrossRef]
17. Gunning, P.J.; Hills, C.D.; Carey, P.J. Accelerated carbonation treatment of industrial wastes. *Waste Manag.* **2010**, *30*, 1081–1090. [CrossRef]
18. Leben, K.; Motlep, R.; Konist, A.; Pihu, T.; Kirsimäe, K. Carbon dioxide sequestration in power plant Ca-rich ash waste deposits. *Oil Shale* **2021**, *38*, 65–88. [CrossRef]
19. Leben, K.; Mõtlep, R.; Paaver, P.; Konist, A.; Pihu, T.; Paiste, P.; Kirsimäe, K. Long-term mineral transformation of Ca-rich oil shale ash waste. *Sci. Total Environ.* **2019**, *658*, 1404–1415. [CrossRef]
20. Usta, M.C.; Yörük, C.R.; Hain, T.; Paaver, P.; Snellings, R.; Rozov, E.; Uibu, M. Evaluation of New Applications of Oil Shale Ashes in Building Materials. *Minerals* **2020**, *10*, 765. [CrossRef]
21. Gunning, P.J.; Hills, C.D.; Carey, P.J. Production of lightweight aggregate from industrial waste and carbon dioxide. *Waste Manag.* **2009**, *29*, 2722–2728. [CrossRef]
22. Quaghebeur, M.; Nielsen, P.; Horckmans, L.; Van Mechelen, D. Accelerated Carbonation of Steel Slag Compacts: Development of High-Strength Construction Materials. *Front. Energy Res.* **2015**, *3*, 52. [CrossRef]
23. Nielsen, P.; Boone, M.A.; Horckmans, L.; Snellings, R.; Quaghebeur, M. Accelerated Carbonation of Steel Slag Monoliths at Low CO₂ Pressure—Microstructure and Strength Development. *J. CO₂ Util.* **2020**, *36*, 124–134. [CrossRef]
24. Sanjuán, M.Á.; Estévez, E.; Argiz, C. Carbon dioxide absorption by blast-furnace slag mortars in function of the curing intensity. *Energies* **2019**, *12*, 2346. [CrossRef]
25. Ohenoja, K.; Rissanen, J.; Kinnunen, P.; Illikainen, M. Direct carbonation of peat-wood fly ash for carbon capture and utilization in construction application. *J. CO₂ Util.* **2020**, *40*, 101203. [CrossRef]
26. Liu, W.; Teng, L.; Rohani, S.; Qin, Z.; Zhao, B.; Xu, C.C.; Liang, B. CO₂ mineral carbonation using industrial solid wastes: A review of recent developments. *Chem. Eng. J.* **2021**, *416*, 129093. [CrossRef]
27. Affordable. Versatile. Sustainable. Available online: <https://www.enefit.com/technology/power-production> (accessed on 14 February 2022).
28. Okia. Utilitas Tallinn. *Utilitas*. Available online: <https://www.utilitas.ee/en/company/as-utilitas-tallinn/> (accessed on 14 February 2022).
29. Electricity and Heat Production. Available online: https://www.energia.ee/en/ettevottest/tehnoloogia/elektri-ja-sooja-tootmine?tabgroup_1=auvere (accessed on 14 February 2022).
30. Arandigoyen, M.; Bicer-Simsir, B.; Alvarez, J.I.; Lange, D.A. Variation of microstructure with carbonation in lime and blended pastes. *Appl. Surf. Sci.* **2006**, *252*, 7562–7571. [CrossRef]
31. Barnes, P.; Bensted, J. *Structure and Performance of Cements*, 2nd ed.; CRC Press: Boca Raton, FL, USA, 2001. [CrossRef]
32. Horkoss, S.; Escadeillas, G.; Rizk, T.; Lteif, R. The effect of the source of cement SO₃ on the expansion of mortars. *Case Stud. Constr. Mater.* **2016**, *4*, 62–72. [CrossRef]
33. ASTM International. Standard Specification for Coal Fly Ash and Raw or Calcined Natural Pozzolan for Use in Concrete (ASTM C618-19). Available online: <https://www.astm.org/> (accessed on 14 February 2022).
34. Humidity Fixed Points of Binary Saturated Aqueous Solutions: Semantic Scholar. Available online: <https://www.semanticscholar.org/paper/Humidity-Fixed-Points-of-Binary-Saturated-Aqueous-Gree-span/9a90c8e8fb71c152ae3bacf9904e6c761cdf9de7> (accessed on 14 February 2022).
35. Fernandezbertos, M.; Simons, S.; Hills, C.; Carey, P. A review of accelerated carbonation technology in the treatment of cement-based materials and sequestration of CO₂. *J. Hazard. Mater.* **2004**, *112*, 193–205. [CrossRef]

36. Pizzol, V.D.; Mendes, L.M.; Savastano, H., Jr.; Frías, M.; Davila, F.J.; Cincotto, M.A.; Tonoli, G.H.D. Mineralogical and microstructural changes promoted by accelerated carbonation and ageing cycles of hybrid fiber–cement composites. *Constr. Build. Mater.* **2014**, *68*, 750–756. [CrossRef]
37. Cui, H.; Tang, W.; Liu, W.; Dong, Z.; Xing, F. Experimental study on effects of CO₂ concentrations on concrete carbonation and diffusion mechanisms. *Constr. Build. Mater.* **2015**, *93*, 522–527. [CrossRef]
38. Mohamed, M.F.; Nor, A.M.; Suhor, M.F.; Singer, M.; Choi, Y.S.; Nešić, S. Water Chemistry for Corrosion Prediction in High Pressure CO₂ Environments. *Corrosion* **2011**, NACE-11375.
39. Fang, Y.; Chang, J. Microstructure changes of waste hydrated cement paste induced by accelerated carbonation. *Constr. Build. Mater.* **2015**, *76*, 360–365. [CrossRef]
40. Liu, X.; Feng, P.; Cai, Y.; Yu, X.; Yu, C.; Ran, Q. Carbonation behavior of calcium silicate hydrate (CSH): Its potential for CO₂ capture. *Chem. Eng. J.* **2022**, *431*, 134243. [CrossRef]
41. Nejad, F.M.; Tolouei, M.; Nazari, H.; Naderan, A. Effects of calcium carbonate nanoparticles and fly ash on mechanical and permeability properties of concrete. *Advances in Civil Engineering. Materials* **2018**, *7*, 651–668. [CrossRef]
42. Usmany, Y.; Putranto, W.A.; Bayuseno, A.P.; Muryanto, S. Crystallization of calcium carbonate (CaCO₃) in a flowing system: Influence of Cu²⁺ additives on induction time and crystalline phase transformation. *AIP Conf. Proc.* **2016**, *1725*, 20093. [CrossRef]
43. Shih, Y. Thermal degradation and kinetic analysis of biodegradable PBS/multiwalled carbon nanotube nanocomposites. *J. Polym. Sci. Part B Polym. Phys.* **2009**, *47*, 1231–1239. [CrossRef]
44. Nam, S.-Y.; Seo, J.; Thriveni, T.; Ahn, J.-W. Accelerated carbonation of municipal solid waste incineration bottom ash for CO₂ sequestration. *Geosystem Eng.* **2012**, *15*, 305–311. [CrossRef]
45. Um, N.; Nam, S.-Y.; Ahn, J.-W. Effect of accelerated carbonation on the leaching behavior of Cr in municipal solid waste incinerator bottom ash and the carbonation kinetics. *Mater. Trans.* **2013**, *54*, 1510–1516. [CrossRef]
46. Khawam, A.; Flanagan, D.R. Solid-state kinetic models: Basics and mathematical fundamentals. *J. Phys. Chem. B.* **2006**, *110*, 17315–17328. [CrossRef] [PubMed]
47. Nikulshina, V.; Gálvez, M.; Steinfeld, A. Kinetic analysis of the carbonation reactions for the capture of CO₂ from air via the Ca(OH)₂–CaCO₃–CaO solar thermochemical cycle. *Chem. Eng. J.* **2007**, *129*, 75–83. [CrossRef]
48. Monkman, S.; Shao, Y. Assessing the carbonation behavior of cementitious materials. *J. Mater. Civ. Eng.* **2006**, *18*, 768–776. [CrossRef]
49. European Commission. Outcome of Proceedings. Circular Economy in the Construction Sector. Available online: <https://data.consilium.europa.eu/doc/document/ST-14653-2019-INIT/en/pdf> (accessed on 14 March 2022).
50. European Commission. European Green Deal: Commission Proposes to Boost Renovation and Decarbonisation of Buildings. Available online: https://ec.europa.eu/commission/presscorner/detail/en/IP_21_6683 (accessed on 14 March 2022).
51. European Commission. Construction Products Regulation Acquis. Internal Market, Industry, Entrepreneurship and SMEs. Available online: https://ec.europa.eu/growth/sectors/construction/construction-products-regulation-cpr/acquis_en (accessed on 14 March 2022).
52. Carbon8 Systems. Available online: <http://www.c8s.co.uk/> (accessed on 12 April 2022).
53. Carbon-Negative Concrete. CarbiCrete. Available online: <http://www.carbcrete.com/> (accessed on 12 April 2022).
54. Carbstone. VITO. Available online: <https://vito.be/en/carbstone> (accessed on 12 April 2022).
55. Telesca, A.; Marroccoli, M.; Montagnaro, F.; Tomasulo, M.; Valenti, G.L. Enhancement of selectivity toward ettringite during hydrothermal processes on fluidized bed combustion wastes for the manufacture of preformed building components. *RSC Adv.* **2015**, *5*, 101887–101893. [CrossRef]
56. Telesca, A.; Calabrese, D.; Marroccoli, M.; Valenti, G.L.; Montagnaro, F. Study of the hydrothermal treatments of residues from fluidized bed combustors for the manufacture of ettringite-based building elements. *Fuel Process. Technol.* **2014**, *126*, 188–191. [CrossRef]
57. Li, X.; Chen, Q.; Huang, K.; Ma, B.; Wu, B. Cementitious properties and hydration mechanism of circulating fluidized bed combustion (CFBC) desulfurization ashes. *Constr. Build. Mater.* **2012**, *36*, 182–187. [CrossRef]
58. Ohenoja, K.; Tanskanen, P.; Wigren, V.; Kinnunen, P.; Körkkö, M.; Peltosaari, O.; Österbacka, J.; Illikainen, M. Self-hardening of fly ashes from a bubbling fluidized bed combustion of peat, forest industry residuals, and wastes. *Fuel* **2016**, *165*, 440–446. [CrossRef]